Research paper

Gas retention in an HMX-based explosive (LX-14)

4 2 0

Michael L. Hobbs*†, Michael J. Kaneshige**, William W. Erikson*, and Kevin T. Miers***

*Engineering Sciences Center, Sandia National Laboratories, Albuquerque, NM, USA
 Phone: 010+1+505−844−5988
†Corresponding author: mlhobbs@sandia.gov

**Energetics Components Center, Sandia National Laboratories, Albuquerque, NM, USA

***US Army Armament Research, Dev. & Engineering Center, Picatinny Arsenal, NJ, USA

Abstract

In previous work, we found that the nitroplasticizer in the HMX-based explosive PBX 9501 played a crucial role in cookoff, especially when predicting response in larger systems[1]. We have recently completed experiments with a similar explosive, LX-14, that has a relatively nonreactive binder. We expected the ignition times for LX-14 to be longer than PBX 9501 since PBX 9501 has a more reactive binder. However, our experiments show the opposite trend. This paradox can be explained by retention of reactive gases within the interior of LX-14 by the higher strength binder resulting in faster ignition times. In contrast, the binder in PBX 9501 melts at low temperatures and does not retain decomposition gases as well as the LX-14 binder. Retention of reactive gases in LX-14 may also explain the more violent response in oblique impact tests[2] when compared to PBX 9501.

Keywords: PBX 9501, LX-14, cookoff, sealed, vented, binder-effects

1. Introduction

The explosive LX-14 is composed of 95.5 wt% octahydro-1,3,5,7-tetranitro-1,3,5,7-tetrazoncine (HMX) with a 4.5 wt% Estane binder (a polyurethane thermoplastic). This explosive reacted violently in several slow cookoff experiments involving a Tube-launched, Optically-tracked, Wirelessly-guided (TOW) devices[3),4)]. LX-14 also reacted violently when subjected to an oblique impact test[2]. In the impact tests, the LX-14 response was more violent than a similar test with PBX 9501, which contains nominally the same amount of HMX (95 wt% vs 95.5 wt%). The primary difference between LX-14 and PBX 9501 is the binder composition. The binder in LX-14 is 4.5% Estane. The binder in PBX 9501 is 2.5% Estane with 2.5% nitroplasticizer (NP) consisting of a 50/50 wt% eutectic mixture of bis (2,2-dinitropropyl)-acetal (BDNPA) and bis (2,2-dinitropropyl)-formal (BDNPF).

Tarver and Tran[5] studied decomposition of numerous explosives composed of HMX and various binders, including LX-14 and PBX 9501. These two explosives were modeled by using an endothermic binder reaction for the Estane and an exothermic reaction for the BDNPA/F.

Tarver and Tran concluded that endothermic binders lengthen the time-to-explosion and exothermic binders shorten the time-to-explosion, although the data did not support this conclusion for LX-14 and PBX 9501. Only one experiment was done with LX-14, which gave similar ignition times as pure HMX. The PBX 9501 ignition times were also similar to pure HMX.

We believe that the similar ignition time for PBX 9501 and pure HMX in Tarver and Tran's one-dimensional time-to-explosion (ODTX) experiment[5),6)] may have been caused by migration of the NP to the highly conductive aluminum anvils that confine the explosive. In highly pressed PBX 9501, the binder thermally expands more than the HMX crystals. At elevated temperatures, the binder flows to the edge of the experiment where the binder energy is dissipated quickly by the conductive aluminum. The PBX 9501 ignition time is then dominated by the HMX kinetics. We have visually observed binder extrusion from highly pressed PBX 9501 in the Sandia Instrumented Thermal Ignition Experiment (SITI) using a borescope[1].

In the current paper, we present new vented and sealed
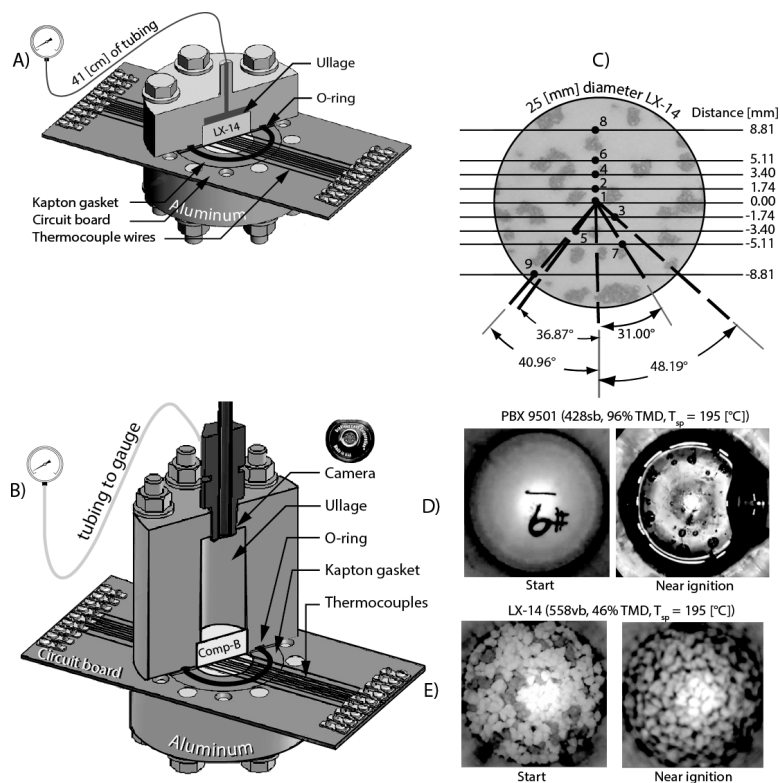
Figure 1 SITI schematic with A) small expansion gap and B) large head space showing borescope camera. C) Cross-section of LX-14 in the SITI apparatus showing thermocouple locations. Borescope images at the beginning and near ignition for D) PBX 9501 and E) LX-14.

SITI experiments of LX-14 and compare these results to PBX 9501. We also present a new LX-14 cookoff model to predict thermal ignition of LX-14. This model considers a small amount of adsorbed gas (moisture) and two additional decomposition reactions. One of these reactions is pressure dependent. All of the reactions use distributed activation energies. The β-δ polymorphic phase change for HMX is accounted for thermodynamically by using an effective capacitance method and normally distributing the reaction enthalpy near the phase change temperature.

Kinetic parameters as well as thermal conductivity for LX-14 were determined using the SITI experiments. The model is validated using ODTX data from Lawrence Livermore National Laboratory[5] as well as cookoff data of a TOW device from the US Army[4]. Uncertainty in the model was determined with a Latin Hypercube Sampling (LHS) analysis.

2. Experimental

The SITI experiments were used to measure the effects of density, excess gas volume (ullage), and confinement (venting vs. sealing) on cookoff of LX-14 with set point temperatures ranging from 190–205 °C (463–478 K). These experiments were used to determine the density and temperature dependent thermal conductivity of LX-14 and to parameterize a simple chemistry mechanism used to predict ignition time.

The ODTX and TOW experiments were used as validation experiments for the LX-14 cookoff model since neither of these experiments were used to obtain model parameters. The ODTX confinement has held at a constant temperature of 220°C (493 K) until ignition

occurred after about 15 min. In contrast, the TOW devices were slowly heated in an oven until ignition occurred after about 23 h from the start of the experiment.

2.1 SITI experiments

Figures 1A and 1B show a schematic of SITI with different ullage volumes. The ullage is either filled with prills for the low-density experiments or is empty for the higher density experiments, as shown in Figure 2A. The empty ullage is modeled as a radiation enclosure. Internal thermocouple junction locations are shown in Figure 1C. The outside temperatures of the confining aluminum cylinders were ramped from room temperature to a set point temperature in 10 min, then held at the set point temperature until ignition.

Pressures were measured with a tube connecting the ullage to a pressure transducer. A borescope was used in several SITI experiments to visually observe differences between heated LX-14 and PBX 9501 as shown in Figures 1D and 1E. The PBX-9501 experiment shows a black liquid that is thought to be the NP extruded to the edge of the explosive as it approaches ignition. In contrast, the LX-14 only shows discoloration as it approaches ignition.

Tables 1–3 give details about each of the SITI experiments such as theoretical maximum density (TMD), set point temperature, ullage volume, and ignition time. The ullage includes the gas volume in the pressure tubing as well as the gas volume above and below the explosive. The run numbers in Tables 1–3 are appended with either "s", "v", or "vb" representing sealed, vented, and vented experiments with a borescope, respectively. SITI experiments were used to determine thermal conductivity
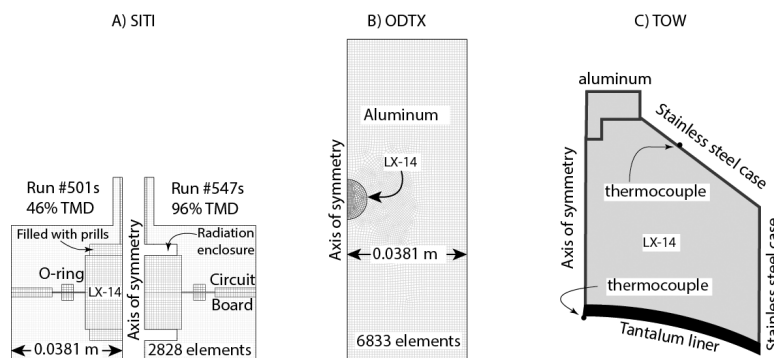
Figure 2 Schematic for A) SITI, B) ODTX, and C) TOW experiments.

Table 1 SITI LX-14 runs with bulk density 859±4 [kg·m^{-3}] (46% TMD)[a,b,c].

Run #	Date	V_{ullage} [cm^3]	T_{sp} [K]	$1000/T$ [K^{-1}]	t_{ign} [s]
501s	9/21/16	0.08	478.2	2.09	2477
502v	9/22/16	0.08	478.2	2.09	4614
503s	9/22/16	0.08	468.2	2.14	4418
504v	9/28/16	0.08	468.2	2.14	10311
506s	9/30/16	0.08	463.2	2.16	6151
508v	10/12/16	0.08	463.2	2.16	20110
554vb	3/29/17	19.6	463.3	2.16	21450
558vb	4/14/17	19.6	468.3	2.14	10482

[a] External temperature ramped from 294.5 ± 1.3 [K] to T_{sp} in 600 [s].

[b] Free gas (ullages or headspace) are filled with prills, except run 554vb and 558vb, where the top ullage is not completely filled.

[c] V_{ullage} includes gas volume in both headspace and pressure tubing.

Table 2 SITI LX-14 runs with bulk density 1548±1 [kg·m^{-3}] (84% TMD)[a,b,c].

Run #	Date	V_{ullage} [cm^3]	T_{sp} [K]	$1000/T$ [K^{-1}]	t_{ign} [s]
548s	3/10/17	2.9	463.25	2.16	5035
549s	3/14/17	2.9	468.29	2.14	3708
550s	3/16/17	2.9	478.27	2.09	2357
551s	3/20/17	4.2	463.25	2.16	5575
552s	3/22/17	4.3	468.26	2.14	3973
553v	3/24/17	4.2	468.26	2.14	4271
560s	5/18/17	4.2	478.24	2.09	2517

[a] External temperature ramped from 293.6±1.6 [K] to T_{sp} in 600 [s].

[b] Free gas (ullage or headspace) is modeled as a radiation enclosure.

[c] V_{ullage} includes gas volume in both headspace and pressure tubing.

Table 3 SITI LX-14 runs with bulk density 1783±8 [kg·m^{-3}] (96% TMD)[a,b,c].

Run #	Date	V_{ullage} [cm^3]	T_{sp} [K]	$1000/T$ [K^{-1}]	t_{ign} [s]
545s	3/3/17	2.9	463.26	2.16	5073
546s	3/7/17	2.9	468.26	2.14	3611
547s	3/9/17	2.9	478.26	2.09	2089
555v	3/31/17	4.4	463.25	2.16	5332
556v	4/5/17	4.3	468.26	2.14	3768
557v	4/7/17	4.4	478.27	2.09	2235

[a] External temperature ramped from 292.2±0.8 [K] to T_{sp} in 600 [s].

[b] Free gas (ullage or headspace) is modeled as a radiation enclosure.

[c] V_{ullage} includes gas volume in both headspace and pressure tubing.

at various densities as well as parameters for a simple cookoff model using both sealed and vented SITI data. Thermal conductivity and reaction parameters were chosen to match temperature histories, pressure histories, and ignition times.

2.2 ODTX validation experiment

Figure 2B shows a schematic with the computational mesh for the ODTX validation experiment. The ODTX experiment consisted of a 0.0127 m diameter sphere of LX-14 that was confined between two 0.0762 m diameter aluminum cylinders with a hemisphere machined into both cylinders to accommodate the explosive. A copper ring was plastically deformed in a groove machined into the anvils near the explosive edge and provided confinement. The cylinders were heated to a prescribed 220°C, giving a constant temperature boundary condition for the one-dimensional experiment. Tarver and Tran[5] reported ignition after about 15 min with a constant boundary temperature of 220. Only one ODTX experiment for LX-14 was reported.

2.3 TOW validation experiments

Al-Shehab et al.[3),4)] presented temperatures of the oven, the outer case, and the tantalum liner from three slow cookoff tests of a TOW devices in a cylindrical body with mock masses. The oven air was heated from ambient temperature to 410 K in 1.4 h, then held at this temperature for 6.1 h, then ramped at 3.3 K/s until ignition occurred. For the three tests, ignition occurred at 22.0 h, 22.7 h, and 22.4 h. Al-Shehab et al.[3),4)] started their calculations after the initial temperature ramp and soak since relatively little chemistry occurs during this time. In the current work, we report all temperatures including the temperature during the initial ramp and soak.

Figure 2C shows a schematic of the TOW device, which consists of a Tantalum liner on the bottom, and a stainless-steel case surrounding the LX-14. A hollow aluminum plug was attached to the top of the TOW device. Standard material properties were used for the nonreactive materials. A response thermocouple was placed on the stainless-steel case and the tantalum liner as indicated in Figure 2C.

There is a temperature lag between the oven air temperature and the response thermocouples located on the TOW. The temperature lag is caused by placement of

Table 4   LX-14 ignition model[a].

Energy conservation	$\rho_b C_b \dfrac{\partial T}{\partial t} = \nabla \cdot (k \nabla T) + \Sigma_{i=1,3} r_i h_{ri} M_{w,i}$	(1)
Mechanism	$(H_2O)_a \xrightarrow{1} H_2O$	(2)
	$HMX\ (C_4H_8N_8O_8) \xrightarrow{2} 4N_2 + 3.6H_2O + 2.2CO_2 + 0.2CH_4 + 1.6C$ or, $HMX \xrightarrow{2} 10G + 1.6C$ P dependent, gas-phase dominates.	(3)
	$HMX\ (C_4H_8N_8O_8) \xrightarrow{3} 4N_2 + 3.6H_2O + 2.2CO_2 + 0.2CH_4 + 1.6C$ or, $HMX \xrightarrow{3} 10G + 1.6C$ P independent, condensed-phase dominates.	(4)
Rates	$r_1 = A_1 \exp\left(\dfrac{-E_1 + \zeta\sigma_1}{RT}\right) [H_2O]$	(5)
	$r_2 = A_2 \left\{ 1 + 0.5 \left(1 + \tanh\dfrac{[T - T_m]}{\Delta T_m}\right) \xi \right\} \left(\dfrac{P}{P_o}\right)^{n2} T^{-1} \exp\left(\dfrac{-E_2 + \zeta\sigma^2}{RT}\right) [HMX]$	(6)
	$r_3 = A^3 \left\{ 1 + 0.5 \left(1 + \tanh\dfrac{[T - T_m]}{\Delta T_m}\right) \xi \right\} T^{-1} \exp\left(\dfrac{-E_3 + \zeta\sigma_3}{RT}\right) [HMX]$	(7)
Species conservation	$\dfrac{d[(H_2O)a]}{dt} = -r_1; \ \dfrac{d[H_2O]}{dt} = r_1; \ \dfrac{d[HMX]}{dt} = -r_1 - r_2;$ $\dfrac{d[G]}{dt} = 10\,(r_1 + r_2); \dfrac{d[C]}{dt} = 1.6\,(r_1 + r_2)$	(8)
Distribution parameter[b], ζ	$P_1 = \dfrac{[H_2O]}{\omega_{H2Oa}\rho b,o / Mw_{H2Oa}}; \ P_2 = P_3 = \dfrac{[HMX]}{\omega_{HMX}\rho_{b,o}/Mw_{HMX}}$	(9)
Pressure	$P = znRT_{ave}/V_g; \ z = 1 + X\exp(\beta X); X = \dfrac{nk\Sigma x_i k_i}{vg\,(T_{ave} + \theta)^\alpha};$ $n = \iiint ([H_2O] + [G])\,dV; \ T_{ave} = \dfrac{\iiint CT dv}{\iiint \rho C dv}; \ V_g = \iiint \phi dV;$ $\phi = 1 - S_f \rho_{c,o}\,(1 - \phi_o)/\rho_c; \ S_f = \dfrac{([(H_2O)a]Mw_{H2O} + [HMX]Mw_{HMX} + [C]Mw_C)}{\rho b,o}$ $\rho_c = \rho_{c,o}\,[1 - 0.00031(T - T_o)], \text{ when } T \leq T_{\beta\,to\,\delta}$ $\rho_c = \rho_{c,o}\,\{[1 - 0.00031(T - T_o)] - 0.067\}, \text{ when } T > T_{\beta\,to\,\delta}$	(10)

[a]Nomenclature and model parameters are given in Table 5.

[b]ζ = norminv(P_i), where "norminv" is the inverse of the standard normal cumulative distribution function that has a mean of 0 and a standard deviation of 1.

the TOW in a complex three-dimensional geometry, which is not shown in the current work. Radiation flux boundary conditions are applied to the aluminum, stainless-steel, and tantalum surface to match the lag between the measured oven air temperature and the measured response thermocouples.

Emissivity of the aluminum, stainless-steel, and tantalum were assumed to be 0.1, 0.1, and 0.2, respectively. A convective boundary condition with a convective coefficient of 3 $Wm^{-2}K^{-1}$ was applied to all of the surfaces except the tantalum surface, which had a convective coefficient of 120 $Wm^{-2}K^{-1}$. The higher convective coefficient was chosen to better match the temperature lag between the oven temperature and the temperature measured on the surface of the tantalum.

3. Engineering model

Table 4 describes a simple ignition model for LX-14 and includes the conductive energy equation, the reaction mechanism, rate equations, species conservation equations, distribution parameter describing reaction progress, and auxiliary equations used to calculate pressure. Table 5 gives nomenclature and model parameters. A single energy equation is solved with a source term for reaction chemistry. The momentum equation is not solved explicitly, however, pressure is

determined using a low Mach flow assumption wherein pressure is assumed to be spatially constant, but changes in time due to temperature changes and chemical decomposition.

The reaction mechanism begins with desorption of a small amount of water (0.5 wt%). The binder does not react in this mechanism; however, the HMX decomposes into equilibrium products via two separate reactions. One of these reactions is dominated by the gas-phase, and the other is dominated by the condensed phase. The kinetics for these reactions are nearly the same. For example, they have the same pre-exponential factor, steric factor, activation energy, and distribution parameter. The only difference is that one of the reactions is multiplied by a pressure ratio raised to the 1/2 power. For vented reactions, these two rates are made the same by setting the pressure exponent to zero. The HMX decomposition reactions are also accelerated by a factor of 100 when the HMX melts. The melt acceleration term is given in curly brackets in Equations (6) and (7).

All three reaction steps use normally distributed activation energies that are distributed with respect to the extent of reaction. For the water desorption model, the positive distribution parameter mimics a decelerating reaction that is representative of a drying process. The negative distribution parameter for the HMX

Table 5 Nomenclature and model parameters.

Symbols	Description	Value	Units
$Ln(A_1)$, $Ln(A_2)$, $Ln(A_3)$,	Natural logarithm of the pre-exponential factors	35, 35, 35	$Ln(s^{-1}K^{-n})$
α	BKW constant	0.5	K^{-1}
β	BKW constant	0.298	none
β_V	Thermal expansion coefficient	0.000131	$(m^3/m^3)K^{-1}$
C	Specific Heat	below 250 K: 919 above 700 K: 2406 250 to 700 K: $92.93+3.305\times T,K$	$Jkg^{-1}K^{-1}$
$C_{eff,\ \beta\ to\ \delta}$	Effective capacitance for β to δ phase change using $h_{latent,\ \beta-\delta}$	441 K: 1550 444 K: 12560 447 K: 1570	$Jkg^{-1}K^{-1}$
$C_{eff,\ HMX\ melt}$	Effective capacitance for HMX melting phase change using $h_{latent,\ melt}$	527 K: 1835 530 K: 80511 533 K: 1854	$Jkg^{-1}K^{-1}$
C	Carbon from HMX decomposition	Symbol used in mechanism	none
C_b	Bulk specific heat	See "C" above	$Jkg^{-1}K^{-1}$
$\Delta T_{\beta-\delta}$	Mush zone for β-δ phase transition	3	K
ΔT_m	Mush zone for HMX melt	1	K
ε	Surface emissivity	0.2 (aluminum, stainless−steel), 0.1 (tantalum)	none
E_1/R, E_2/R, E_3/R	Activation energies divided by R	25500, 17450, 17450	K
ϕ	Gas volume fraction	Field variable	m^3/m^3
ϕ_o	Initial gas volume fraction	$1-\rho_{bo}/\rho_{co}$	m^3/m^3
[G]	Gas concentration	Initially 0	$kgmol/m^3$
[H_2O_a]	Adsorbed water concentration	Initially $\omega_{H2Oa}\times\rho_{bo}/M_{w,H2Oa}$	$kgmol/m^3$
[H_2O]	Desorbed water concentration	Initially 0	$kgmol/m^3$
$h_{f,i}$ where $i=$ H_2O_a, H_2O_g, G, C, HMX	Heat of formation of species	-285.8×10^6, -241.8×10^6, -175.1×10^6, 0, 75×10^6	$Jkgmol^{-1}$
$h_{latent,\beta-\delta}$	Latent enthalpy for β-δ phase change	33000	$J\ kg^{-1}$
$h_{latent,m}$	Latent enthalpy for HMX melt	236000	$J\ kg^{-1}$
i	i^{th} reaction	1, 2, 3	none
$\varkappa$	BKW constant	10.5×10^{-3}	$\text{Å}^{-3}m^3kgmol^1K^\alpha$
$\Sigma x_i k_i$	Average BKW covolume factor	447	Å^{-3}
κ	Thermal conductivity	$\begin{cases} k_\beta & T\leq441 \\ k_\beta+\dfrac{k_\delta-k_\beta}{447-441}(T-441) & 441<T<447 \\ k\delta & 447\geq T \end{cases}$	$Wm^{-1}K^{-1}$
$k\beta$	Thermal conductivity of LX-14 with β-HMX.	$\begin{cases} 0.35 & \rho_{b,0}\geq1779 \\ 0.0003030\rho_{b,0}-0.18909 & 1548\leq\rho_{b,0}<1779 \\ 0.0002305\rho_{b,0}-0.07689 & 854\leq\rho_{b,0}<1548 \\ 0.12 & \rho_{b,0}<854 \end{cases}$	$Wm^{-1}K^{-1}$
$k\delta$	Thermal conductivity of LX-14 with δ-HMX.	$\begin{cases} 0.25 & \rho_{b,0}\geq1779 \\ 0.0001732\rho_{b,0}-0.05805 & 1548\leq\rho_{b,0}<1779 \\ 0.0001513\rho_{b,0}-0.02421 & 854\leq\rho_{b,0}<1548 \\ 0.105 & \rho_{b,0}<854 \end{cases}$	$Wm^{-1}K^{-1}$
m_1, m_2, m_3	Steric factor for reactions 1 to 3	0, −1, −1	K^{-1}
$M_{w,i}$, where $i=$ H_2O_a, H_2O_g, HMX, G, C	Molecular weight of species	18, 18, 296.2, 27.6, 12	kg/kgmol
n	Moles of gas	Field variable (Eqn. 10)	kgmol
n_2	Pressure exponent for reaction 2	0.5	none
normsinv	Inverse of st. normal distribution	function	none
P	Pressure	Initially 0	MPa (psig)
P_i (where $i=1,3$)	Progress of reaction 1−3	Field variable (Eqn. 9)	kgmol/kgmol
P_{max}	Maximum pressure before failure	SITI: not reached, ODTX: 186, TOW: 2.1	MPa
P_o	Initial pressure	0.08 SITI, 0.1 ODTX, 0.1 TOW	MPa
θ	BKW constant	6620	K
ρ	Bulk density	Field variable	kgm^{-3}
$\rho_{b,o}$	Initial bulk density	SITI: Tables 1−3 ODTX: 1780 TOW: 1734	kgm^{-3}
ρ_c	Condensed density	Field variable (Eqn. 10)	kgm^{-3}
$\rho_{c,o}$	Initial condensed density (TMD)	1860	kgm^{-3}
r_1, r_2, r_3	Rate of reaction 1, 2, and 3	Field variable (Eqns. 5−7)	s^{-1}
R	Gas constant	8314	$J\ kgmol^{-1}K^{-1}$
σ_1/R, σ_2/R, σ_3/R	Distribution parameter	2500, −1000, −1000	K
S_f	Reacted solid fraction	Field variable	kg/kg
T	Temperature	Field variable	K
T_{ave}	Average gas temperature	Global variables	K
$T_{\beta-\delta}$	β to δ phase change temperature	444 (normal distribution over 441−447)	K
T_{melt}	HMX melting temperature	530 (normal distribution over 527−533)	K

Table 5 (continued)

Symbols	Description	Value	Units
T_o	Initial temperature	SITI: Tables 1: 3 ODTX: 300 K TOW: 289	K
T_{sp}	Set point temperature	SITI: See Tables 1−3 ODTX: 493 TOW: unspecified	K
t_{ign}	Time-to-ignition	SITI: See Tables 1−3 ODTX: 936 when $T_{sp} = 493$ [K] TOW: 79200, 81890, 82800	s
V	Gas volume	Global variable from Eqn. 10	m^3
V_{EM}	Volume of the energetic material	SITI molding powder: 15.82×10^{-6} SITI pressed pellets: 12.87×10^{-6} ODTX: 1.073×10^{-6} TOW: not specified	m^3
V_{ullage}	Volume of ullage	SITI: see Tables 1−3 ODTX: 0.068×10^{-6} TOW: not specified	m^3
ω_{H_2Oa}	Mass fraction of adsorbed water	Initially 0.005	kg/kg
ω_{HMX}	Mass fraction of HMX	Initially $0.955 - \omega_{H_2Oa}$	kg/kg
X	Part of BKW equation	Defined in Eqn. 15	none
x_i, where i = N_2, H_2O, CO_2, CH_4	Gas mole fractions for HMX reaction	0.4, 0.36, 0.22, 0.02	mol/mol
ξ	normsinv	Field variable	none
ζ	Melt rate acceleration factor	100	none
z	Compressibility	Global variables (Eqn. 15)	none

decomposition reactions accelerates the reactions with respect to the extent of decomposition. For the HMX reactions, the activation energy is high at the start of reaction, then gets lower as the reaction proceeds.

The model uses an effective capacitance model for both the β-to-δ polymorphic phase change as well as melting of the HMX. Table 5 gives the effective capacitances for these phase changes as triangular distributions centered around the phase change temperature. Rather than using this sharp triangular distribution, we use a more smooth, normal distribution to get better convergence of our model, with essentially the same results as the triangular distribution.

The reaction enthalpies are calculated using Hess's law using the heat of formation of the reactants and products for each of the reactions. For most problems of interest, the ideal gas law is sufficient to calculate the pressure. However, the ODTX experiment is rated for 153 MPa and a real gas equation of state is needed. The BKW-EOS[7] is used for high pressure calculations.

4. Results

Figure 3 shows ignition times and temperatures for the SITI, ODTX, and TOW experiments. Figure 3A shows the ignition times for LX-14 in the SITI apparatus as a function of density and temperature. In Figure 3A, the LX-14 data is plotted using circles. The black circles are for the sealed experiments, and the white circles are for the vented experiments. The time-to-ignition for the vented experiments is much larger than the sealed experiments. However, the difference in ignition times for vented and sealed LX-14 experiments is much less than that for the PBX 9501 experiments. The PBX 9501 experiments are plotted as small squares with the gray squares representing the sealed experiments and the white

squares representing the vented experiments.

Figure 3A shows longer ignition times for the PBX 9501 SITI experiments when compared to the LX-14 experiments for all densities. The PBX 9501 shows a large effect of venting for all densities, although the effect is less for the 96% TMD experiments. In contrast, the LX-14 shows a small venting effect at densities of 46% TMD, and no effect of venting for the 84% TMD and 96% TMD SITI experiments. We believe the absence of confinement effects (vented vs sealed) is due to retention of the reactive gases within the LX-14.

Figure 3B show the predicted and measured internal temperatures for various SITI runs that are labeled in Figure 3A. The left-hand image in Figure 3B shows a comparison between predicted internal temperatures and pressure for SITI runs 547s, 550s, and 501s. Each of these runs have the same set point temperature and only differ by density. Clearly, ignition is delayed for the lower density explosives. The predicted delay is caused by less gas decomposition products resulting in lower internal pressures, which lowers the reaction rates.

The middle and right-hand images in Figure 3B present experimental evidence for ignition delay between LX-14 and PBX 9501. Each of the experiments plotted in these figures has the same set point temperature. The delay in ignition time may be caused by less pressure within the respective explosives lending support to our hypothesis that LX-14 retains reactive gases better than PBX 9501.

Figure 3C presents validation data for our LX-14 model. The left-hand image shows a comparison between the sealed LX-14 model with $n_2 = 0.5$ and the vented LX-14 model with $n_2 = 0$. The data matches the results using the vented model. Conclusions regarding the model are difficult with only one data point. We suggest more data be acquired with the ODTX experiment for better model
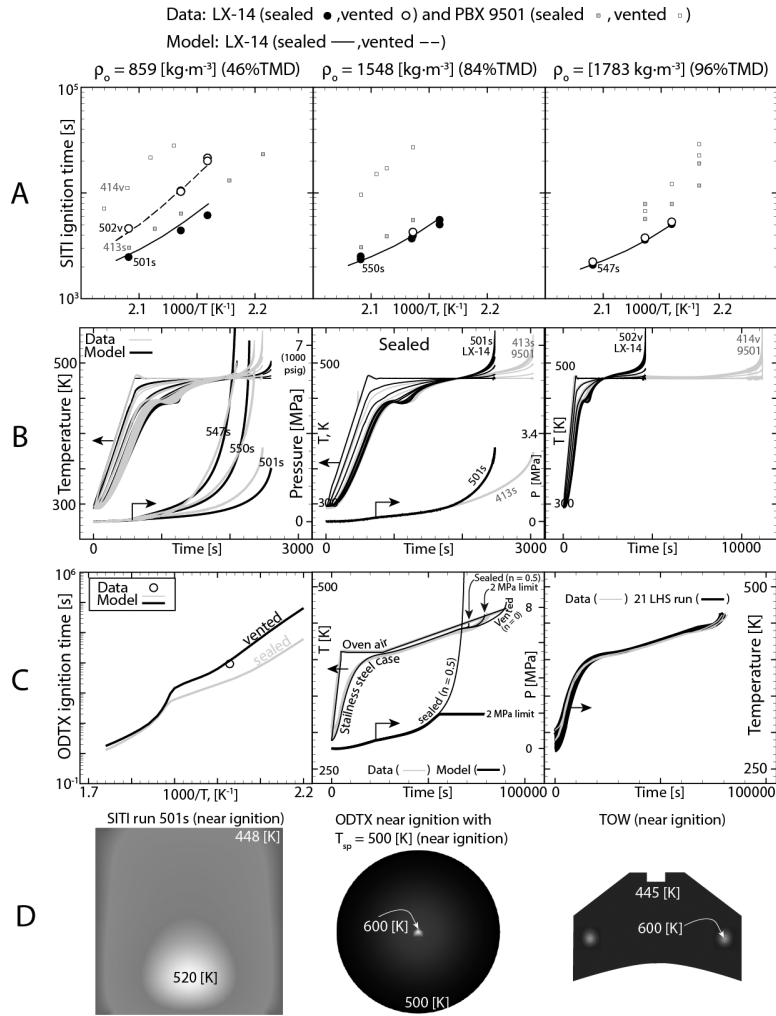
Figure 3 A) SITI ignition times, B) SITI temperature and pressure profiles, C) ODTX ignition times and TOW temperature and pressures, and D) temperature contours near ignition for SITI, ODTX, and TOW.

evaluation. One problem with the ODTX experiment is the small size of the sample and the difficulty in measuring the excess gas volume or void.

The right two images in Figure 3C give the predicted and measured temperature of the TOW stainless-steel case. The middle image in Figure 3C also shows the measured and predicted temperature of the air in the oven. The temperature difference between the case and the oven air is the lag caused by complex three-dimensional heat transfer. The TOW devices are placed within cylinders and also have various masses attached to the devices that are not modeled.

Rather than model the TOW configuration in three dimensions, we have applied both radiative and convective boundary conditions on the aluminum plug on top of the TOW, stainless-steel casing, and tantalum liner. The emissivity of the aluminum and stainless-steel surfaces was set to 0.2 and the emissivity of the tantalum was set to 0.1. The convective coefficient was set to 3 $Wm^{-2}K^{-1}$ for the aluminum and stainless-steel surfaces and 120 $Wm^{-2} K^{-1}$ on the tantalum surface. The higher convection coefficient was used to match the initial temperature lag between the thermocouple located on the tantalum and the oven temperature.

The middle image in Figure 3C shows the oven and stainless-steel temperatures. The measured oven and stainless-steel temperatures are from three runs with nominally the same boundary condition. The measured temperatures are shown as gray lines. The oven temperature is specified in the model and is represented by the black line. The stainless-steel surfaces are predicted using the parameters in Table 5. Three predictions of the surfaces are shown in the middle image assuming 1) no pressure limit, 2) 2 MPa pressure limit, and 2) vented. The predicted ignition times for these three cases are 19.7 h, 22.0 h, and 25.1 h, respectively. The measured ignition times for the three tests were 22.0, 22.4, 22.7 h. The pressure within the LX-14 in the TOW tests was not measured. However, the measured ignition times were within the vented and sealed predictions. Limiting the pressure to 2 MPa (300 psig) gives about the correct ignition times.

The right image in Figure 3C shows the uncertainty in the model predictions. We used 21 Latin Hypercube Sample (LHS) runs to determine the response of the model with uncertainty in 20 of the input parameters. Each of these runs are plotted as black lines in the right image of Figure 3C. The three experimental responses are plotted as light grey lines.

LHS uncertainty analysis is an efficient Monte-Carlo technique to extract uncertainty in the model response[8]. In the current paper, 18 parameters (e.g. ρ_{bo}, T_o, P_o, ω_{H2Oa},

$h_{latent,\beta-\delta}$, $\Delta T_{\beta-\delta}$, $h_{latent,m}$, ΔT_m, k, C, r_1, r_2, ξ, P_{max}, h_{conv} (tantalum and stainless-steel), and ε (tantalum and stainless-steel) were varied by plus or minus 5% assuming a uniform distribution of the input parameters. The phase change temperatures ($T_{\beta-\delta}$, T_m) were varied between 442−446 K for the β-to-δ phase change and between 528−532 K for the HMX melting point.

The images in Figure 3D show the predicted ignition location in the SITI, ODTX, and TOW experiments. The predicted ignition locations in the SITI run 501s was slightly off center. The predicted ignition locations in the ODTX run was in the center of the sphere. The predicted ignition locations in the TOW experiment was near the bottom right side of the LX-14. Better predictions could be made using the complete three-dimensional geometry.

5. Conclusions

In an effort to validate our observation that the NP in PBX 9501 played a significant role in cookoff, we performed several experiments with LX-14, which contained nominally the same amount of HMX, had an Estane binder, but no NP. We discovered that the LX-14, without the NP, ignited sooner than the PBX 9501.

We have simulated our LX-14 SITI cookoff experiments by solving the conductive energy equation with a source for chemistry. The chemical mechanism included drying and two HMX decomposition steps. One of the HMX decomposition steps was assumed to be pressure dependent, and was parameterized using low-density LX-14 SITI data in both sealed and vented configurations. The model was validated using various SITI, ODTX, and TOW experiments.

We performed both sealed and vented SITI cookoff experiments of LX-14 with densities of 46%TMD, 84%TMD, and 96%TMD. The effect of venting was notable in the 46%TMD experiments, although the venting effect was much less than in our previous experiments with PBX 9501. We did not observe an appreciable effect of venting with our 84%TMD and 96%TMD runs, leading us to conclude that the reactive gases are retained within the LX-14 during cookoff.

References

1) M. L. Hobbs, M. J. Kaneshige, and W. W. Erikson, Combust. Flame, 173, 132−150 (2016).
2) G. Parker, M. Holmes, E. Heatwole, L. Vaughn, R. Broilo, and P. Dickson, "Oblique Impacts with PBX 9404, LX-14, LX-10, and Aged PBX 9501: Fiscal Year 2016 Skid Testing Results," Los Alamos Laboratory Report LA-UR-16−26795, Los Alamos (2016).
3) N. Al-Shehab, E. L. Baker, N. Peterson, D. Hunter, L. Pitts, K. Huddleston, E. Colvin, and M. Steinberg, Proc. Insensitive Munitions & Energetic Materials Technology Symposium, San Diego (2013).
4) N. Al-Shehab, E. L. Baker, N. Peterson, D. Hunter, L. Pitts, K. Huddleston, E. Covin, and M. Steinberg, Proc. Insensitive Munitions and Energetic Materials Technology Symposium, Rome (2015).
5) C. M. Tarver and T. D. Tran, Combust. Flame, 137, 50−62 (2004).
6) R. R. McGuire and C. M. Tarver, Proc. Seventh Symposium (International) on Detonation, 56−64, U.S. Naval Academy, Annapolis (1981).
7) M. L. Hobbs and M. R. Baer, Shock Waves, 2, 177−187 (1992).
8) M. D. McKay, W. J. Beckman, and W. J. Conover, Technometrics, 21, 239−245 (1979).